Growth of Highly Fluorescent Polyethylene Glycol- and Zwitterion-Functionalized Gold Nanoclusters

Fadi Aldeek,[†] M. A. Habeeb Muhammed,[‡] Goutam Palui,[†] Naiqian Zhan,[†] and Hedi Mattoussi[†,*]

[†]Department of Chemistry and Biochemistry, Florida State University, 95 Chieftan Way, Tallahassee, Florida 32306, United States, and [‡]Department für Physik und CeNS, Ludwig-Maximilians-Universtität München, Amalienstraße 54, D-80799 München, Germany

ABSTRACT

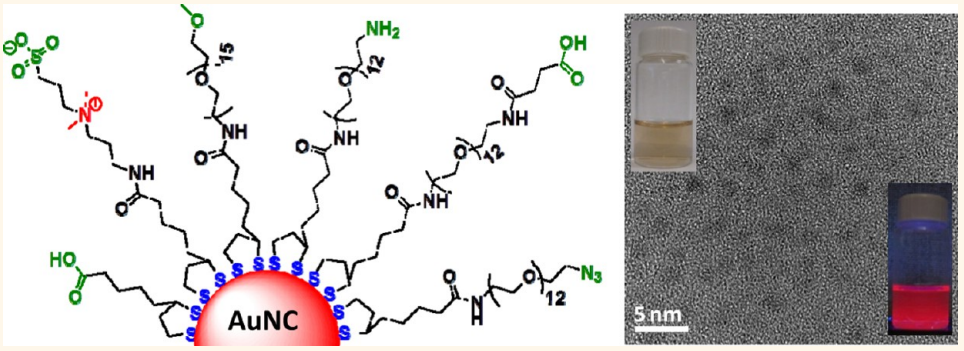

We have prepared and characterized a new set of highly fluorescent gold nanoclusters (AuNCs) using one-step aqueous reduction of a gold precursor in the presence of bidentate ligands made of lipoic acid anchoring groups, appended with either a poly(ethylene glycol) short chain or a zwitterion group. The AuNCs fluoresce in the red to near-infrared region of the optical spectrum with emission centered at ~750 nm and a quantum yield of ~10−14%, and they exhibit long fluorescence lifetimes (up to ~300 ns). Dispersions of these AuNCs exhibit great long-term colloidal stability, over a wide range of pHs (2−13) and in the presence of high electrolyte concentrations, and a strong resistance to reducing agents such as glutathione. The growth strategy further permitted the controlled, *in situ* functionalization of the NCs with reactive groups (*e.g.*, carboxylic acid or amine), making these nanoclusters compatible with common and simple-to-implement coupling strategies, such as carbodiimide chemistry. These properties combined make these fluorescent NCs greatly promising for use in various imaging and sensing applications where NIR and long-lived excitations are desired.

KEYWORDS: metal nanoclusters · fluorescence · ligand · reduction · functionalization

Confinement of electrons within a metallic nanostructure in a size regime comparable to the Fermi wavelength of electrons (*ca.* 0.7 nm for gold and silver) provides materials referred to as metal clusters or nanoclusters (NCs).[1,2] They exhibit *molecule-like* properties, including size- and composition-dependent optical properties.[1−5] Gold nanoclusters (AuNCs), in particular, have generated a tremendous interest because they offer a challenging fundamental problem, namely, understanding the growth and stability of such structures and the effects of charge carrier confinements on their optical and spectroscopic properties.[1,2,5−10] Due to their ultrasmall size and photostability, Au clusters can be used as fluorescent probes and can potentially compete with quantum dots and fluorescent proteins. Furthermore, fluorescent AuNCs do not face the stigma of potential cytotoxicity (not fully justified) encountered by luminescent quantum dots (QDs).[11−14] Growth of Au clusters with size-tunable photoluminescence (PL) from the near-infrared (NIR) to the ultraviolet (UV) has been reported.[15] Their applications range from developing optical and electronic devices[16−19] to the sensing of small molecules, metal ions, proteins, and nucleic acids.[15,20,21]

Various methods have been developed for the synthesis of AuNCs, which can be broadly classified into four categories: (1)

* Address correspondence to mattoussi@chem.fsu.edu.

Received for review December 18, 2012 and accepted February 9, 2013.

Published online February 09, 2013
10.1021/nn305856t

direct reduction of gold precursor(s), or a bottom-up approach,[22,23] (2) core etching of metallic nanoparticles (NPs) into smaller size clusters, or a top-down approach,[24−26] (3) size focusing of a group of clusters with varying numbers of core atoms to a thermodynamically most stable cluster,[27−29] and (4) conversion of an as-prepared cluster into a larger one by cap exchange with thiol-terminated ligands (*e.g.*, Au_{11} to Au_{25} and A_{55} to Au_{75}).[30,31] Among those synthetic routes, the bottom-up approach has been more commonly used; here, the gold precursor is first treated with suitable "protecting groups" known as ligands, followed by reduction of the metal *via* a chemical, photochemical, or sonochemical process.[32−35] The commonly used ligands include thiol-appended molecules,[36−40] dendrimers,[41−43] peptides,[22,44] proteins,[45,46] DNA,[47] and polymers.[24] The final NCs are composed of metallic cores, each consisting of a finite number of gold atoms, surface-capped with a layer of organic molecules (ligands). Ligands that present vastly different architectures and affinities to the metal have been used in these growth schemes, which can affect the final size and stability of the clusters along with their photophysical properties.[18] Among the various ligands used for the stabilization of NCs, multithiol-based ligands (with at least two coordinating groups) provide enhanced colloidal stability to the NCs. For example, Chang and co-workers reported the synthesis of water-dispersible dihydrolipoic acid (DHLA)-capped AuNCs using a strategy relying on core etching of nanoparticles.[26] They first prepared hydrophobic AuNPs (∼5.5 nm) stabilized with didodecyldimethyl ammonium bromide (DDAB) in toluene, followed by gold ion-induced etching of the NP core in organic solvent and ligand exchange with DHLA to obtain water-dispersible luminescent NCs with an average core diameter of ∼1.5 nm. These clusters emit in the red to near-infrared region of the optical spectrum with a rather low quantum yield (QY ∼2%). They then used liposome complexes to deliver these clusters to cells (human aortic endothelial cells and endothelial progenitor cells) and found that the intracellular fluorescence lasted for at least 28 days.[12]

Nienhaus and co-workers reported a one-pot synthesis of water-soluble red fluorescent DHLA-capped AuNCs by direct reduction of a gold precursor using sodium borohydride; here too, a rather low QY (∼0.6%) was reported.[38] Recently, Tan and co-workers reported the use of a multidentate thioether (pentaerythritol tetrakis 3-mercaptopropionate-terminated poly(methacrylic acid), PTMP-PMAA), combined with one-step reduction of a gold precursor in aqueous solution, to grow red-emitting AuNCs with a QY of ∼5%. These clusters were used in selective labeling of cancer K562 and normal cord blood mononuclear cells.[40] More recently, the same group reported the use of thioether polymer (PTMP)-terminated polyvinyl acetate ester (PVAc) to prepare blue-emitting AuNCs in organic solution (THF) with high PL QY (∼25%).[39]

Despite the progress made in the past decade in developing various routes to grow luminescent AuNCs, their integration into biological systems was rather slow due to several limitations, including (1) reduced colloidal stability in the presence of excess salts and pH changes, (2) reduced stability against thiol-containing reducing agents, and (3) lack of control over the number of reactive groups on the NCs, making further controlled functionalization with desired biomolecules nearly impossible. Thus, new synthetic routes to grow luminescent AuNCs with high QY and enhanced colloidal stability over a broad range of conditions are still needed.

We have previously reported the use of one-phase aqueous growth of spherical gold nanoparticles (AuNPs) with sizes ranging from 2 to 20 nm, using modular ligands made of polyethylene glycol (PEG) appended with lipoic acid (LA) anchoring groups.[48] Here, the NP size was controlled by varying the molar ratio between the gold precursor and the ligands. These AuNPs exhibited great colloidal stability over a broad range of conditions, including high electrolyte concentration (up to 2 M NaCl), pH changes from strongly acidic to alkaline, and the presence of excess dithiothreitol (DTT).[48] More recently, a few groups reported the design and synthesis of zwitterionic (ZW) ligands appended with either lipoic acid or dopamine ligands (*e.g.*, sulfobetaine-terminated DHLA or dopamine) and demonstrated their use for capping core−shell CdSe-ZnS QDs and Fe_2O_3 NPs.[49−53] These zwitterionic ligands provided NPs with smaller hydrodynamic size.

Here, we build on those findings and report the use of one-phase growth to prepare a series of fluorescent AuNCs stabilized with PEG- or zwitterion-appended lipoic acid ligands. The resulting NCs fluoresce in the far red to near-infrared region of the spectrum (peak centered at ∼750 nm) with high quantum yield (up to 14%), have long excitation lifetimes, and exhibit remarkable colloidal stability. In addition, the synthetic scheme allowed the *in situ* insertion of controllable numbers of reactive groups (namely, amine or carboxyl groups) on the NC surfaces, which can permit further covalent coupling of the clusters to a variety of target biomolecules.

RESULTS AND DISCUSSION

The present approach was guided by the ability of the one-phase growth route to provide LA-PEG-stabilized AuNPs with discrete size control over the range spanning 2−20 nm, as described in ref 48. We were also motivated by the recent developments in the synthesis of sulfobetaine-modified lipoic acid (LA-zwitterion, LA-ZW) ligands reported by Lequeux and co-workers and Kim and co-workers, have provided QDs with good colloidal stability and reduced hydrodynamic size.[51,52]

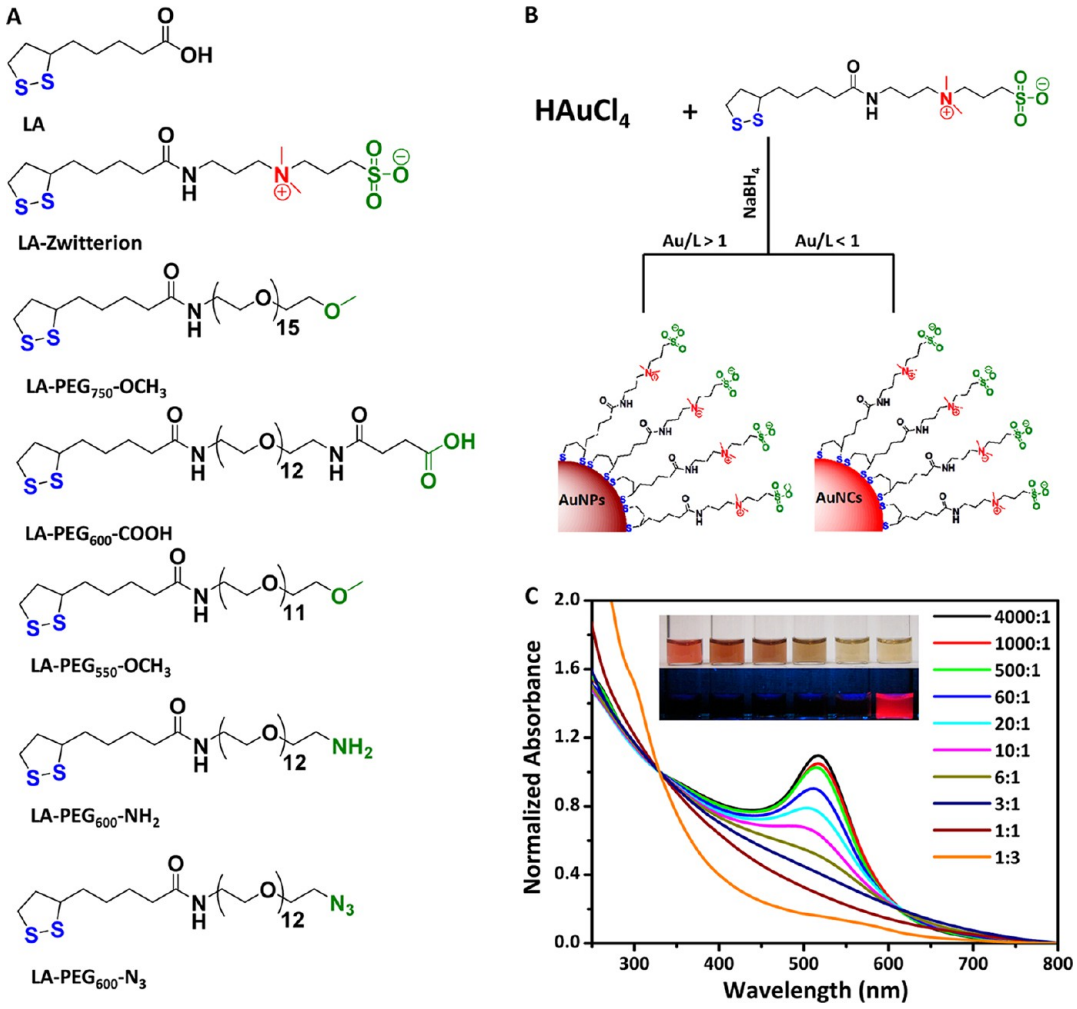

Figure 1. (A) Chemical structures of the ligands used for the synthesis and functionalization of AuNCs. (B) Schematic representation of the AuNP *versus* AuNC growth using LA-ZW ligand. (C) Normalized UV−vis absorption spectra for several AuNPs and NCs grown using various molar Au-to-LA-ZW ratios. Inset in C shows images collected under white light and UV irradiation for a set of AuNP and NC dispersions in water. Change in the dispersion color reflects the effects of NP size on the plasmonic absorption. Only the cluster dispersion is fluorescent when irradiated with a hand-held UV lamp (λ_{ex} = 365 nm).

In a preliminary experiment we applied the one-phase growth using LA-ZW ligands (instead of LA-PEG) to prepare a set of AuNPs where size was controlled by varying the Au:ligand molar ratios (Figure 1B).[48] And indeed, we found that LA-ZW-capped AuNPs, with continuous progression in the absorption features, similar to those reported using LA-PEG-OCH_3, can be prepared (Figure 1C).[48]

Here, we wanted to extend those findings to the growth of a new set of ultrasmall Au nanocrystals (Au nanoclusters) that are fluorescent, colloidally stable, and readily functionalized with reactive groups (*e.g.*, COOH, NH_2, or N_3). In addition to commercially available lipoic acid, four LA-PEG-based ligands, LA-PEG_{750}-OCH_3, LA-PEG_{550}-OCH_3, LA-PEG_{600}-NH_2, and LA-PEG_{600}-COOH, along with LA-ZW, were used for the cluster growth;[51,54−56] growth using LA provided control/reference samples. The chemical structures of these ligands are shown in Figure 1A. The synthesis of AuNCs was carried out by direct reduction of a gold precursor in the presence of the ligands using excess $NaBH_4$ at pH ∼11 (see schematics in Figure 1B).

We first optimized the growth of AuNCs prepared with LA-PEG_{750}-OCH_3 or LA-ZW by varying the relative molar concentrations of the ligands, $NaBH_4$ and $HAuCl_4$. Overall, we found that growth of fluorescent AuNCs with homogeneous size can be achieved only in the presence of excess ligands and sodium borohydride (see Supporting Information, Figures S1, S2, and S3). A broad red emission spanning the far red to NIR region of the spectrum characterizes all samples. Furthermore, even though the emission location was essentially unaffected by the ligand molar excess, its intensity strongly depended on the Au-to-ligand ratio, with the brightest emission obtained for Au:ligand = 1:3 and the lowest intensity for Au:ligand = 1:1. We also found that ∼2 molar equivalent of $NaBH_4$ (with respect to gold) was necessary to grow fluorescent AuNCs. This value is similar to what has been reported by Nienhaus and co-workers for NCs prepared using commercially

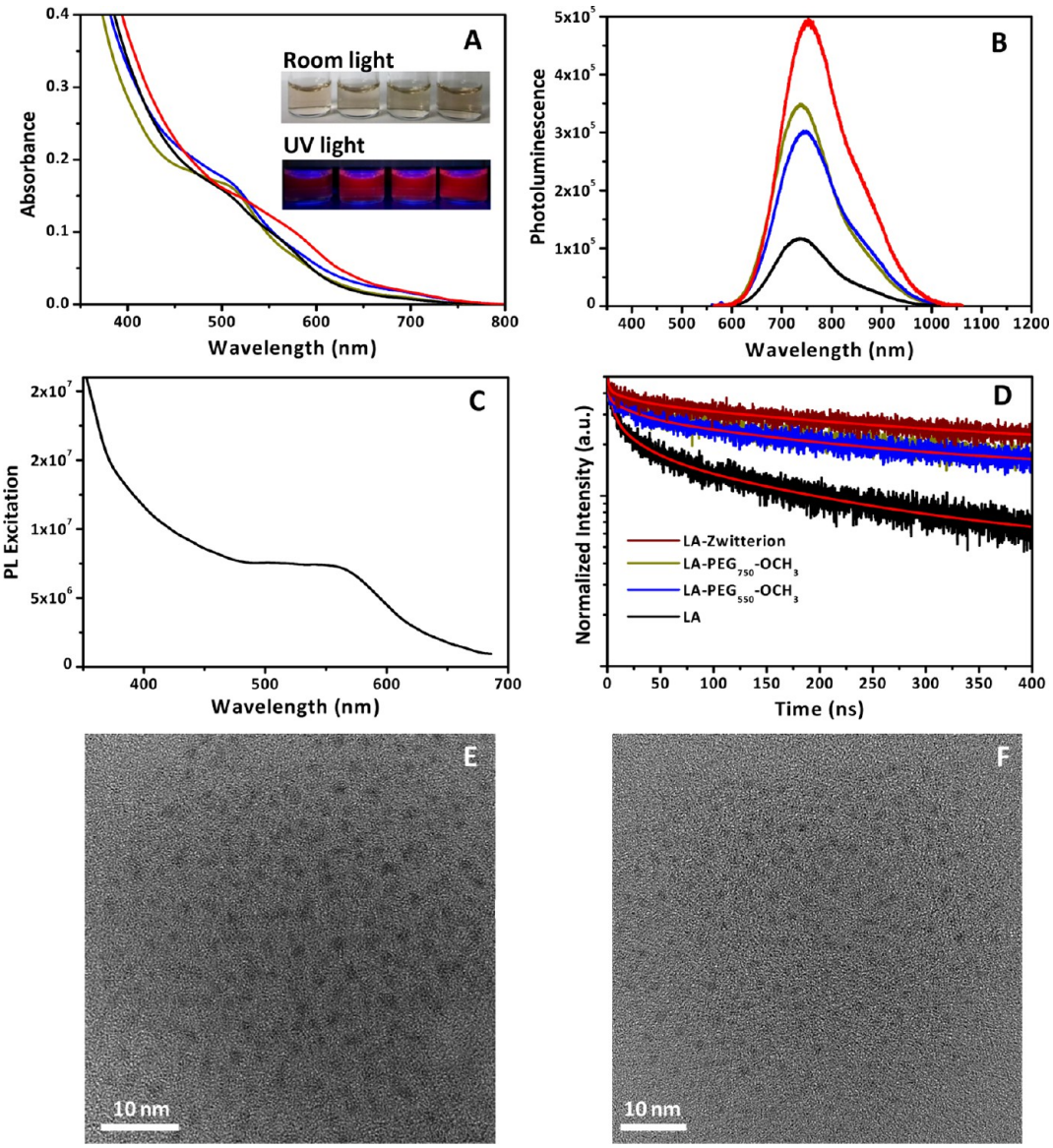

Figure 2. (A) UV−vis absorption and (B) PL spectra of the AuNCs; shown are NCs grown using LA (black line), LA-PEG_{550}-OCH_3 (blue line), LA-PEG_{750}-OCH_3 (dark yellow line), and LA-ZW (crimson line). Inset image shows the corresponding (from left to right) photographs of AuNCs prepared using the above four ligands under room and UV light exposure (using a hand-held UV lamp, λ_{exc} = 365 nm). The Au:$NaBH_4$:ligand molar ratio used for the synthesis was 1:2:3. (C) Excitation spectrum of LA-ZW-capped AuNCs. (D) Time-resolved fluorescence decay curves of LA-, LA-PEG_{550}-OCH_3-, LA-PEG_{750}-OCH_3-, and LA-ZW-capped AuNCs and the corresponding fits using a three-exponential decay function (red line); additional details on the fit are provided in the Supporting Information. (E) TEM images of LA-PEG_{750}-OCH_3- and (F) LA-ZW-capped AuNCs. Fluorescence spectra were generated using λ_{ex} = 550 nm.

available lipoic acid.[38] Finally, the absorption spectra collected from samples prepared with LA-PEG ligands showed a small peak at ~510 nm, although a spectrum with less clearly defined features was measured for the clusters prepared using lower ligand concentrations (*i.e.*, Au:ligand = 1:1, see Supporting Information, Figure S1). Next we systematically investigated the influence of the nature of the ligands on the photophysical properties and structure of the AuNCs, focusing on clusters grown using Au:ligand = 1:3. For this, PEG-free lipoic acid and LA-ZW along with PEGylated LA (inert, LA-PEG_{550}-OCH_3 and LA-PEG_{750}-OCH_3), or mixtures of inert and end-functionalized PEG ligands (*e.g.*, NH_2 or COOH) were used. The absorption spectra of AuNCs prepared with LA and LA-PEG, recorded immediately after the synthesis, are largely similar with continuously decaying curves (Figure 2A). They exhibit a weakly defined band/peak whose position slightly varies with the type of ligand; peak locations at 505, 508, and 512 nm are measured for clusters synthesized in the presence of LA, LA-PEG_{550}-OCH_3, and LA-PEG_{750}-OCH_3, respectively. In comparison, clusters prepared using LA-ZW show a broader and slightly red-shifted absorption peak at 573 nm; the peak is less defined than the one measured for NCs prepared using LA-PEGs. Figure 2B shows that the corresponding photoluminescence spectra

collected using excitation at 550 nm are overall similar, with a broad emission spanning the red to the NIR region of the optical spectrum. The PL maximum slightly varies depending on the ligand, with peaks measured at 737, 747, and 753 nm for LA-PEG_{750}-OCH_3 (and LA), LA-PEG_{550}-OCH_3, and LA-ZW, respectively. The spectra are not affected by the excitation line, even though the overall intensity increases when bluer excitation is used. A representative excitation spectrum, shown in Figure 2C for LA-ZW clusters, indicates that PL excitation tracks the absorption spectrum shown in Figure 2A, with a weakly defined peak at 570 nm. We should stress that the excitation spectra measured for the AuNCs stabilized with the other ligands are similar to the corresponding absorption spectra shown in Figure 2A.

However, the fluorescence intensity is significantly affected by the nature of the ligand used. For instance, the PL quantum yields measured for the various clusters are 3.5% for LA, 9.8% for LA-PEG_{550}-OCH_3, 12.5% for LA-PEG_{750}-OCH_3, and 14% for LA-ZW; these PL yields were calculated using rhodamine 6G as reference. Figure 2A also shows the corresponding photographs of the NC dispersions under white light and UV illumination (using a hand-held UV lamp, with λ_{exc} = 365 nm). Clearly, the LA-AuNCs dispersion shows the weakest emission, while the sample with LA-ZW-AuNCs exhibits the brightest PL. The time-resolved fluorescence decay curves are fitted with a three-exponential decay function for all the prepared clusters.[57] Rather long average lifetimes were measured, with values of 179, 276, 300, and 362 ns for LA, LA-PEG_{550}-OCH_3, LA-PEG_{750}-OCH_3, and LA-ZW, respectively (Figure 2D).

Finally, the structure of the clusters was characterized using high-resolution transmission electron microscopy (HRTEM). The TEM images collected from dispersions of clusters grown in the presence of LA-PEG_{750}-OCH_3 and LA-ZW ligands (Figure 2E, F) show ultrasmall and homogeneous clusters with average diameters of 1.2 $\pm$ 0.4 and 1.3 $\pm$ 0.3 nm, respectively.

Remark. We have tried to characterize our clusters using both electrospray ionization (ESI) and matrix-assisted laser desorption ionization (MALDI) mass spectroscopy to gain insight into their atomic numbers/orders. However, we only measured peaks corresponding to the molecular distribution of the PEG ligand, as we observed for silver nanoclusters (AgNCs) prepared using similar rationales.[58] We believe that this may be due to the inadequacy of the commonly used matrices and the complexity of the ligands used. Most reported clusters were prepared using molecular ligands or proteins where size dispersity is not an issue.

We tested the long-term stability of LA-PEG_{750}-OCH_3- and LA-ZW-capped clusters dispersed in buffers under three different conditions: (1) over a broad pH range, (2) in the presence of large excess salt, and (3) against competition from glutathione (GSH), a natural reducing agent. The data were compared to those collected from LA-capped AuNCs (control).

These tests are highly relevant to the use of these NCs as fluorescent platforms in biology. For example, several biological transformations have been associated with changes in pH. Also, pH can provide a reliable indication for disease progression, including cancer metastasis, chronic fatigue, and depression.[59,60] Moreover, NPs and NCs stabilized with laterally charged ligands (*e.g.*, carboxy- or amine-terminated alkyl ligands) often exhibit nonspecific interactions with the extracellular matrices and serum proteins.[61,62] Similarly, electrolytes influence and control the physical behavior of proteins and nucleic acids.[63−65] Indeed, the average concentration of NaCl in the nucleus of live cells (where genomic DNA is present) varies from 0 to ~150 mM.[64] In addition, the nature of the interactions between these electrolytes and the surface capping layer can affect the NP/NC long-term intracellular stability.

The tripeptide glutathione is a natural, low molecular weight, reducing agent often abundant in mammalian cells (~5 mM concentration). It is an important antioxidant and plays a valuable role in metabolic functions, including amino acid transport, detoxification of cells, and neurotransmission.[66] GSH exhibits strong affinity to AuNPs/AuNCs, due to the presence of thiolate and other reactive groups in its structure,[67] and excess GSH can displace weakly coordinating native ligands, potentially altering the NP/NC colloidal stability and photophysical properties.[68,69] Thus, NC stability in the presence of excess GSH can provide a direct indication of the behavior of our AuNCs in the presence of this and other thiol-containing compounds abundantly present in biological media.

We checked the stability of the AuNCs dispersed in phosphate buffers with pH ranging from 2 to 13 over a period extending up to six months. Figure 3A, B show the fluorescence images of AuNC dispersions capped with LA-PEG_{750}-OCH_3 and LA-ZW in phosphate buffers; samples were irradiated at 365 nm using a hand-held UV lamp. Figure 3C, D show representative PL spectra of LA-PEG_{750}-OCH_3- and LA-ZW-capped NCs freshly prepared, after one month and after three months of storage at 4 °C. The dispersions remained aggregate-free across the full pH range for 10 months of storage. The fluorescence emission was unaffected for dispersions of AuNCs prepared using LA-PEG ligands over the pH range 4−13, while that of dispersions prepared using LA-ZW slightly decreased after 10 months of storage. Nonetheless, at pH = 2 the fluorescence of the clusters prepared using either ligand substantially decreased after 10 months of storage to *ca.* half of their initial values. In contrast, LA-capped AuNCs became unstable shortly after transfer to the acidic buffers (see Supporting Information, Figure S4).

Figure 3E, F show the PL spectra of LA-PEG_{750}-OCH_3- and LA-ZW-AuNCs dispersed in pure PBS buffer

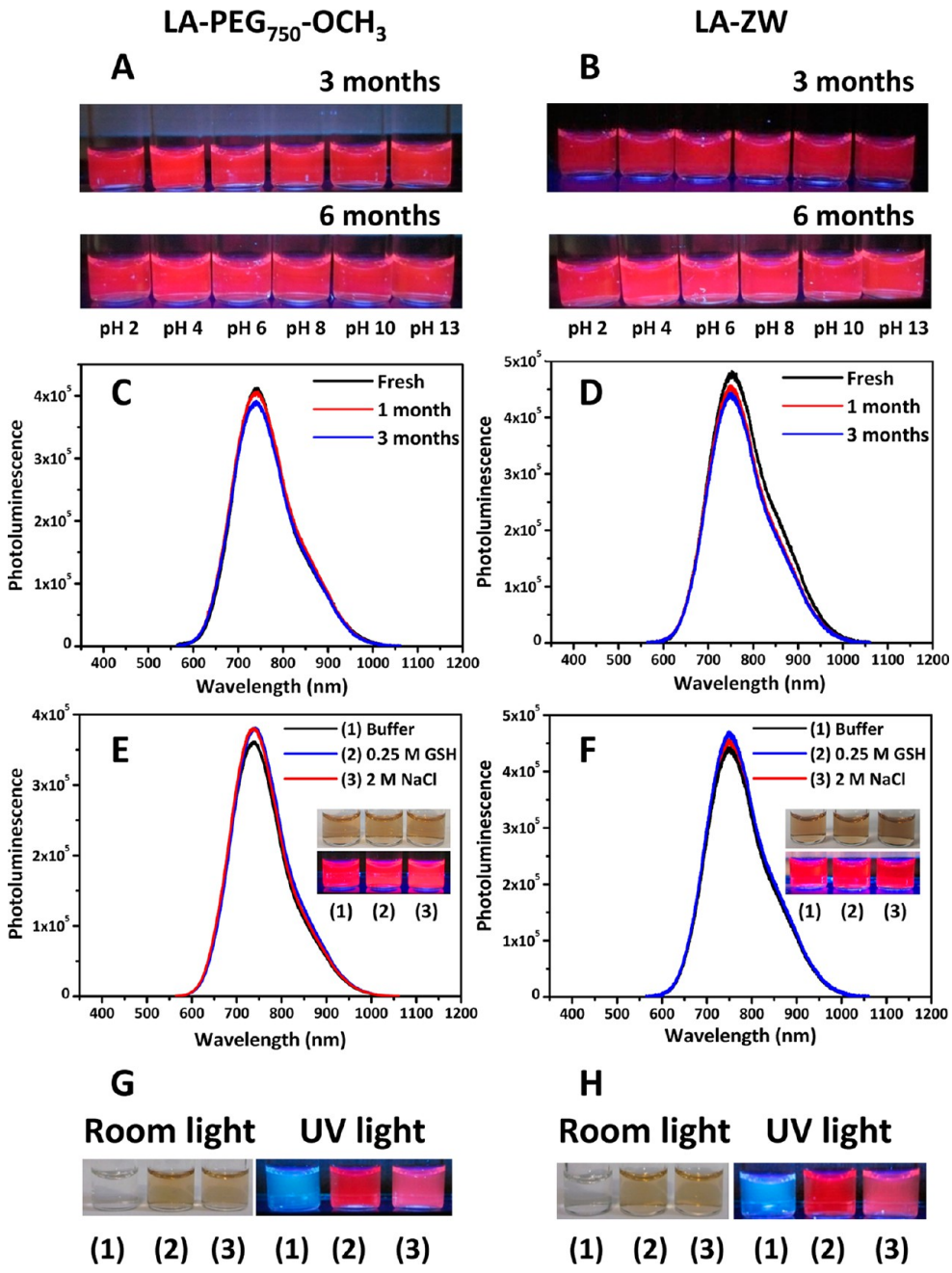

Figure 3. (A) Fluorescence images of LA-PEG_{750}-OCH_3- and (B) LA-ZW-capped AuNCs in buffers at pH ranging from 2 to 13, taken after three and six months of storage. (C) PL spectra of LA-PEG_{750}-OCH_3- and (D) LA-ZW-capped AuNCs freshly prepared, after 1 month and 3 months of storage. (E, F) PL spectra of AuNCs prepared using the above ligands in PBS buffer, PBS buffer containing 0.25M GSH, and PBS buffer containing 2 M NaCl. Inset shows a photograph of the corresponding AuNCs under room and UV light exposure; image taken after 1 day of storage. (G, H) Images under room and UV light exposure: (1) pure DMEM growth media, (2) AuNCs in DI water, and (3) AuNCs in DMEM growth media; images were taken after 1 day of storage. The fluorescence spectra were generated using λ_{ex} = 550 nm.

and in buffer containing either 2 M NaCl or 0.25 M GSH collected after one day of storage. The PL of the clusters under these conditions was unaffected for at least three months of storage, with no measurable change in the peak location or overall intensity. In comparison, the data collected from LA-capped NCs indicate that while exhibiting colloidal stability in the presence of NaCl (2 M), the PL intensity increased by a factor of 2 along with a small red shift (from 737 to 750 nm, see Supporting Information, Figure S4). LA-capped AuNCs became unstable in the presence of GSH and aggregated with time (see Supporting Information, Figure S4).

We also checked the colloidal stability of AuNCs in Dulbecco's modified Eagle growth media (DMEM), commonly used for eukaryotic cell cultures. Here too the LA-PEG- or LA-ZW-capped AuNC dispersions remained stable and aggregate-free after several months of storage (Figure 3G, H). [We should note that the

DMEM growth media itself exhibits a pronounced blue emission (under UV irradiation), which is due to the presence of amino acids bearing aromatic residues such as phenylalanine and tryptophan. This additional contribution alters the overall emission of the clusters dispersed in the media from red to pinkish, as shown in Figure 3G, H.]

The different behaviors exhibited by the clusters prepared with lipoic acid can be attributed to the nature of the ligand. Aggregation in acidic conditions results from protonation of the lateral carboxylate groups on the LA-capped AuNCs in acidic buffers, as has been shown for DHLA-capped QDs; LA is made of a short alkyl chain, and the protonated ligand is naturally hydrophobic.[70] Similarly, the enhanced colloidal stability and increased PL in the presence of excess NaCl in DI water can be attributed to an increase in the packing density of lipoic acid molecules on the NC surface, as recently suggested by Volkert and co-workers for LA-capped AuNPs.[71] This issue is not relevant when PEG- or ZW-appended ligands are used. The effects of added GSH to LA-AuNC dispersions may also be attributed to the reducing nature of GSH (GSH is a proton donor), which protonates the periphery of these NCs, making them less stable. Indeed, the pH of the solution measured after the addition of GSH was ~3.

Finally, we explored the possibility of phase transferring the as-prepared NCs from water to other organic solvents.[58] This is important, as it indicates one's ability to process them in various solution conditions, which potentially expands their utility outside biology. For this, AuNCs initially grown in the presence of LA-PEG_{750}-OCH_3 in water were purified as described above, then divided into equal aliquots and lyophilized. Following complete water removal, 1 mL of water, ethyl acetate, chloroform, THF, acetone, 2-propanol, and acetonitrile were added to the dried clusters, producing homogeneous and fluorescent dispersions of Au clusters with strong emission. The collected image indicates that the PL of the NCs is nearly identical for all solvents tested (Figure 4).

These findings combined clearly confirm that our ligands made of zwitterion- and PEG-modified lipoic (and dihydrolipoic) acid, as bidentate anchoring groups, provide remarkable colloidal stability to the AuNCs over a broad range of stringent conditions, including a high concentration of electrolytes and reducing agents, as well as over a broad pH range. This is attributable to the strong coordination afforded by the anchoring group onto the metal surface combined with the inert nature of the PEG or ZW lateral functions. This makes these materials very promising for use as fluorescent platforms in biology as well as outside biology since these materials can be dispersed and manipulated in, and processed from, water as well as an array of organic solvents.

One of the key features of our synthetic scheme is that it allows the *in situ* introduction of controllable

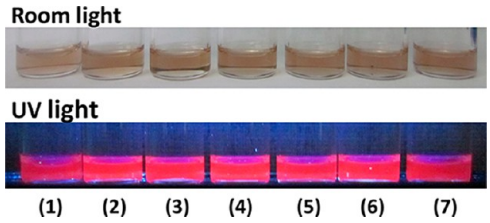

Figure 4. (Top) White light and (bottom) fluorescence images of LA-PEG_{750}-OCH_3-capped AuNCs redispersed in different solvents. The fluorescence image was generated using a hand-held UV lamp (λ_{exc} = 365 nm): (1) water, (2) ethyl acetate, (3) chloroform, (4) THF, (5) acetone, (6) 2-propanol, (7) acetonitrile.

fractions of reactive groups on the cluster surfaces. This is achieved by mixing controlled fractions of reactive ligands (*e.g.*, LA-PEG_{600}-COOH or LA-PEG_{600}-NH_2) with the inert ligands (namely, LA-PEG_{750}-OCH_3 or LA-ZW) during growth.[48,54] Here we used inert-to-reactive molar ratios of 1:0, 0.85:0.15, 0.7:0.3, 0.5:0.5, and 0:1 (additional data are provided in the Supporting Information, Figures S5 and S6). The presence of amine and carboxy groups on the surface of the AuNCs was confirmed by gel electrophoresis. Figure 5A shows that AuNCs prepared with 100% OCH_3 ligands do not exhibit any mobility shift under applied voltage, while AuNCs functionalized with different percentages of COOH or NH_2 migrate toward the anode and cathode, respectively. The mobility shift depends on the fraction of reactive groups used.[54] However, the functionalization of the AuNCs with an azide-terminated ligand could not be achieved during the initial growth, as done for the amine- or carboxy-terminated ligands, because the presence of $NaBH_4$ at high concentrations alters the integrity of azide groups.[72] To introduce azide groups on the cluster surfaces, we instead relied on the rationale used in our previous work, where the reactive ligands were introduced after the growth was arrested (*i.e.*, during the passivation step). For this, a 3-fold molar excess of PEG-azide (*i.e.*, total LA-PEG_{600}-N_3-to-Au molar ratio ~3) was added to the solution and left stirring for 3 h. Side-by-side FT-IR spectra collected for this sample and one for clusters, not subjected to the passivation step (methoxy-terminated), are shown in Figure 5B. A clearly defined band at 2100 cm^{-1} is measured for dispersions of the clusters subjected to the extra passivation step, but not for the control dispersion, which confirms the presence of the azide groups on the cluster surfaces (Figure 5B).

We then checked the compatibility of the resulting AuNCs with amine-to-NHS coupling chemistry. Two dispersions of AuNCs capped with different percentages of amine groups, 30% and 100%, were reacted with 20 equivalents of sulfo-Cy3 NHS ester in PBS buffer (pH = 8.4) for four hours. The resulting AuNC-Cy3 conjugates were then purified from excess free dye and NHS byproduct by size exclusion filtration using a PD10 column. Figure 6A, B show the absorption spectra of

the initial AuNCs (capped with 30% and 100% LA-PEG_{600}-NH_2, respectively) along with spectra of the purified AuNC–dye conjugates. The absorption spectra (raw and deconvoluted) show clear dye contribution observed only for the clusters prepared with mixed ligands (Figure 6), confirming that the coupling between the amines on the NCs and NHS–dye has taken place. The absorption peak of the AuNC–dye conjugates exhibits a small red shift compared to the dye alone from 548 to 553 nm, a feature often observed for dyes conjugated to other molecules.[73] Further analysis of the spectra in Figure 6 shows that the deconvoluted dye absorption tracks the increase in the expected number of amine groups on the NCs when the fraction of LA-PEG_{600}-NH_2 is increased. Indeed, the molar concentration of Cy3 dye extracted from the absorption data using the dye extinction coefficient (162 000 cm^{-1} M^{-1}) measured for AuNCs grown using 100% LA-PEG_{600}-NH_2-capped is 3 times larger than the one measured for AuNCs prepared using a 70:30 mixture of LA-PEG_{750}-OCH_3:LA-PEG_{600}-NH_2. This proves that control over the fraction of functional ligands, introduced during the AuNC growth, can permit eventual control over the amount of molecules (*e.g.*, dyes or proteins) coupled to the clusters. We should, nonetheless, note that though the increase in the amount of bound dyes to the cluster tracked the increase in the fraction of amines introduced during the growth, exact values for the number of dyes per cluster could not be determined. This is primarily due to the lack of an accurate estimate of NC extinction coefficient.

To elucidate the growth mechanism of these NCs, we monitored the time-dependent changes in the UV–vis absorption and emission features under various conditions. We first investigated the interactions between the ligand (here LA-PEG_{750}-OCH_3) and Au precursor alone and after mixing (Figure 7A). The spectra collected for the pure compounds show a weakly defined absorption peak around 330 nm and a more pronounced peak at 290 nm for the ligand and aurate solutions, respectively. Following mixing of the aurate with LA-PEG_{750}-OCH_3 the two peaks rapidly disappeared and an absorption shoulder appeared at 340 nm. The new absorbance at 340 nm decreased progressively with time before saturation was reached within 5 min; this was accompanied by a color change in the solution mixture from light yellow to colorless. When $NaBH_4$ was added, the solution color gradually

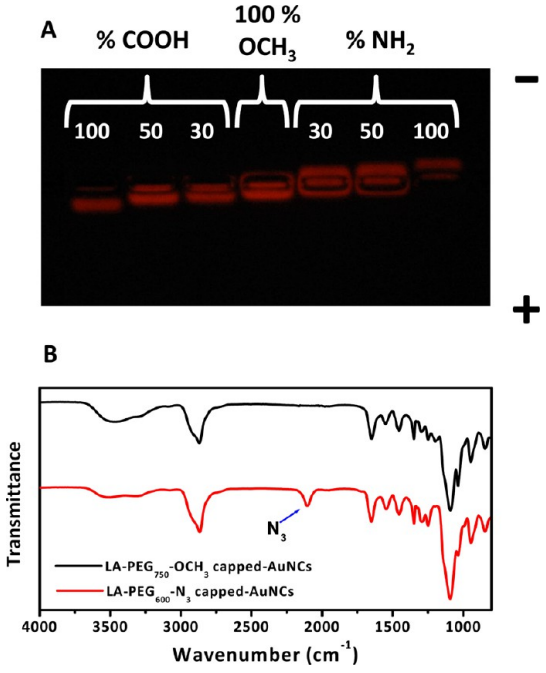

Figure 5. (A) Gel electrophoresis fluorescence image of LA-PEG_{750}-OCH_3-capped AuNCs before and after functionalization with LA-PEG_{600}-COOH and LA-PEG_{600}-NH_2 ligands; the amine and carboxy fractions used are shown. (B) FT-IR spectra of methoxy-functionalized (black line) and azide-functionalized AuNCs (red line). The arrow (at ~2100 cm^{-1}) indicates the azide band observed only for the clusters subjected to extra passivation with LA-PEG_{600}-N_3.

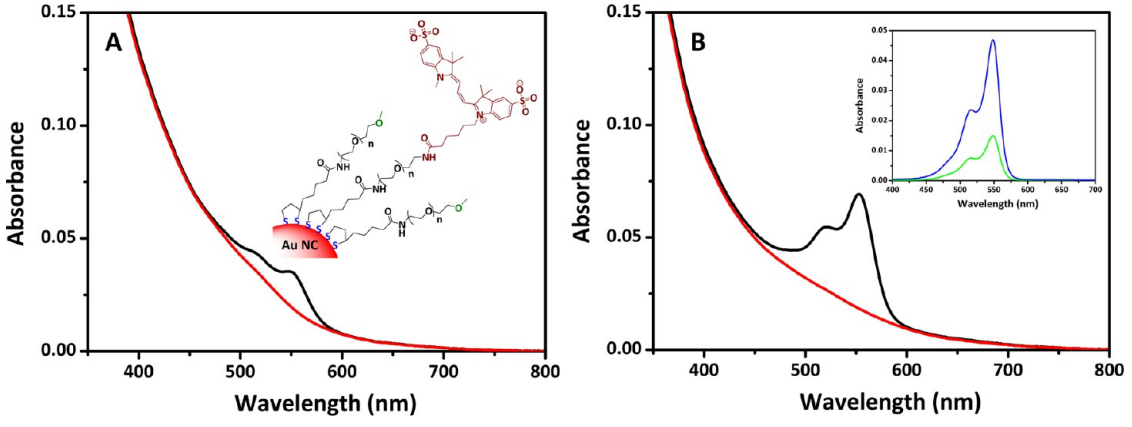

Figure 6. Absorption spectra of AuNCs unconjugated (red line) and conjugated to sulfo-Cy3 (black line): clusters prepared with 30% LA-PEG_{600}-NH_2 (A) and 100% LA-PEG_{600}-NH_2 (B). Inset in (A) shows a representative scheme of sulfo-Cy3 dye conjugated to amine-functionalized AuNCs. Inset in (B) shows the deconvoluted absorption spectra of sulfo-Cy3 for different percentages of LA-PEG_{600}-NH_2 used during the cluster growth: 30% (green line) and 100% (blue line).

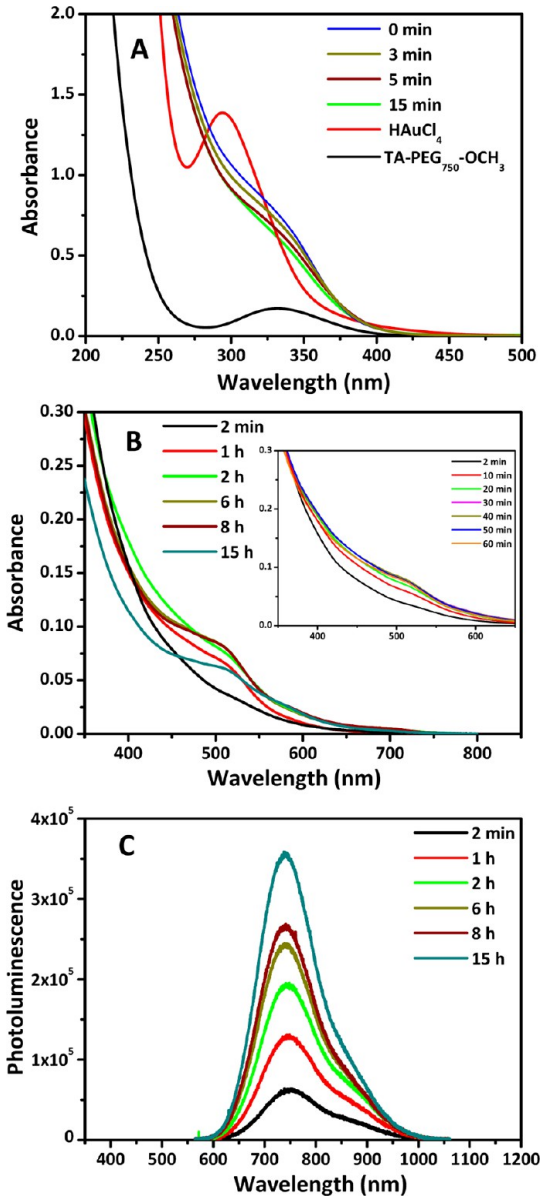

Figure 7. (A) Time-dependent UV−vis absorption spectra for $HAuCl_4$ and LA-PEG_{750}-OCH_3 ligand mixtures (Au:ligand = 1:3, concentrations of the ligand = 1.5 mM, and that of Au = 0.5 mM). Changes in the spectra show the formation of a gold-to-ligand complex. Time-dependent UV−vis absorption (B) and the corresponding fluorescence (C) spectra collected during the cluster growth. The fluorescence spectra were generated using λ_{ex} = 550 nm.

turned light brown, and a featureless continuously decaying absorption spectrum appeared after 2 min (Figure 7B). Then, a broad and weakly defined absorption around 512 nm slowly developed within the first two hours. The absorption peak continued to evolve until saturation was reached after ~15 h (Figure 7B).[48] This gradual transformation was associated with a progressive buildup in the luminescence, as a broad spectrum with a maximum at 737 nm was measured (Figure 7A).

We attribute the weak absorption peak at 330 nm to the disulfide group in the LA-PEG_{750}-OCH_3 ligand; a similar peak is also measured for the lipoic acid alone.[53,74] When the ligand is mixed with the gold chloride, Au(I)-LA-PEG_{750}-OCH_3 metal−ligand complexes are formed due to the interaction of the Au(III) ions with the disulfide group, resulting in the disappearance of the absorption features associated with the ligand and Au precursor separately.[48] At this time, there are no NCs present in the solution, as confirmed by the absence of any characterestic absorption and emission features. After the addition of $NaBH_4$, the solution turns light brown due to the reduction of Au(I)-LA-PEG_{750}-OCH_3 complexes into Au(0) core seeds.[22,75] During this time a group of NCs may be formed, and as the reaction progresses, a single most stable NC is formed accompanied with the appearance of the indicative characterestic absorption and emission features.

Unlike metallic nanoparticles, clusters possess discrete energy levels due to confinement effects when the nanocrystal size becomes ultrasmall; their optical properties are then derived from the electronic transitions between the molecular orbitals (MOs) as predicted by time-dependent density functional theory (TDDFT) calculations of the electronic structures and optical transition of the NCs.[10] The MOs of gold NCs have contributions from the atomic orbitals Au (6sp) and Au (5d) of the metal core and S (3p) of the ligands. MOs formed from sp orbitals make up the sp band, whereas those formed from d orbitals constitute the d band. The absorption features arise due to the transition of electrons between these MOs. These transitions are of one-electron in nature. NIR emission of the NCs may arise from the radiative intraband transition within the sp band across the HOMO−LUMO gap. Both the core and the nature of ligands play a crucial role in determining the absorption and emission properties of the AuNCs, because the number of ligands and metal atoms per individual cluster are comparable.[23,76,77] This may be the reason for the observation of dissimilar absorption features and QY values obtained with different ligands during the NC growth. The core Au metal, with its quantization effect, and the ligand at the surface, with its charge transfer to the metal core, are both responsible for the exciton relaxation involving sp and d interbands.[10] The ligand plays an important role in the fluorescence generation, especially when the ligand possesses electron-rich atoms.[18] According to this, our ligand contribution may play a larger role here, since the photoluminescence of AuNCs is dependent on the nature of the LA-based ligands used in the synthesis.

CONCLUSION

We have developed a one-phase growth strategy to prepare a set of small-size nanocrystals made of gold cores (Au nanoclusters) of 1.2 nm diameter, stabilized with multifunctional ligands made of lipoic acid anchoring groups appended with either poly(ethylene glycol) or zwitterion hydrophilic modules.

The NCs exhibit emission in the far red region of the optical spectrum, with high quantum yield, long fluorescence lifetimes, and a remarkable colloidal and photophysical stability over a wide range of conditions. This synthesis route also permits the insertion of a controllable number of functional groups on the cluster surfaces, simply by introducing the desired molar fraction of the reactive ligand before the metal reduction. This allowed further coupling of these nanoclusters to functional dyes and opens the possibility to conjugate the AuNCs to a variety of biomolecules using common and simple to implement coupling strategies, including carbodiimide, cysteine-maleimide, and click chemistry using target molecules presenting groups such as amine, carboxy, and cyclooctyne. These properties combined make these clusters greatly promising for probing a variety of biological problems, such as protein diffusion in confined cellular compartments, where small size and/or long lifetime excitation are desired (*e.g.,* fluorescence lifetime imaging microscopy, FLIM). These clusters can also provide additional advantages for *in vivo* (deep-tissue) imaging using fluorescence techniques, where far red to IR emission is desired.

EXPERIMENTAL SECTION

Reagents. Gold(III) chloride trihydrate ($HAuCl_4 \cdot 3H_2O$) (99.9%), ±-α-lipoic acid, poly(ethylene glycol) ($M_w \approx 600$), poly(ethylene glycol) methyl ether ($M_w \approx 750$ and 550), methanesulfonyl chloride (99.7%), triphenylphosphine (99%), 4-(*N*,*N*-dimethylamino)pyridine (99%), triethylamine (Et_3N), sodium borohydride ($NaBH_4$), *N*,*N*-dicylohexylcarbodiimide, succinic anyhydride, 1-ethyl-3-(3-dimethylaminopropyl)carbodiimide hydrochloride, *N*-hydroxysuccinimide (98%) (NHS), NaOH, KOH, $NaHCO_3$, organic solvents (THF, $CHCl_3$, *etc.*), salts (such as NaCl, Na_2SO_4, Mg_2SO_4), and rhodamine 6G were purchased from Sigma Chemicals (St. Louis, MO, USA). Sodium azide (99%), *N*,*N*-dimethyl-1,3-propanediamine (99%), and 1,3-propanesultone (99%) were purchased from Alfa Aesar (Ward Hill, MA, USA). Sulfo-Cy3 NHS ester was purchased from Lumiprobe (Hallandale Beach, FL, USA). Deuterated solvents were purchased from Cambridge Isotope Laboratories (Andover, MA, USA). The chemicals and solvents were used as purchased unless otherwise specified. Column purification chromatography was performed using silica gel (60 Å, 230−400 mesh, from Bodman Industries, Aston, PA, USA). PD10 columns were purchased from GE Healthcare (Piscataway, NJ, USA).

Instrumentation. ^{1}H NMR spectra of all compounds were recorded using a Bruker SpectroSpin 600 MHz spectrometer. The optical absorption measurements were carried out using a Shimadzu UV−vis absorption spectrophotometer (UV 2450 model from Shimadzu). The emission and excitation spectra were collected on a Fluorolog-3 spectrometer (HORIBA Jobin Yvon Inc., Edison, NJ, USA) equipped with CCD and PMT detectors; emission spectra were collected using the CCD detector, while excitation scans were collected using the PMT detector. The time-resolved fluorescence decay data were collected using a TCSPC (time correlation single photon counting) system integrated into the same Fluorolog-3. We used a pulsed excitation signal at 440 nm with a repetition rate of 1 MHz, provided by NanoLED-440LH (100 ps, fwhm), while detection was collected on the same PMT detector above. The fluorescence decay traces of the AuNCs emission (limited to a narrow window centered at the peak of the PL spectrum) were analyzed using the above TCSPC system and fitted to a three-exponential function as detailed in ref 57. Samples for transmission electron microscopy (TEM) were prepared by drop casting the AuNC dispersions onto a holey carbon film on a fine-mesh Cu grid (400 mesh) and letting it dry; images were collected using a JEOI-2010 200 kV instrument. For the gel electrophoresis experiments the NC dispersions were first diluted in a 10% glycerol 1× TBE tris borate EDTA (100 mM Tris, 83 mM boric acid, 1 mM EDTA, pH 8.3) loading buffer. Then the aliquots of these dispersions were loaded into 1% agarose gel, and experiments were conducted using a voltage of 7−8 V/cm for 15 min. A Bio-Rad Chemidoc gel imaging system was used to image the gels. FT-IR spectra of the purified AuNCs were collected using a 100 FT-IR spectrometer (PerkinElmer, Waltham, MA, USA). The QY values were determined using the equation $QY_{sample} = (F_{sample}/F_{ref})(A_{ref}/A_{sample})(n_{sample}^2/n_{ref}^2)QY_{ref}$ where *F*, *A*, and *n* are the measured fluorescence (area under the emission peak), the absorbance at the excitation wavelength, and the refractive index of the solvent, respectively. The PL quantum yields were determined relative to rhodamine 6G in ethanol (QY = 94%).[78]

Synthesis of LA-PEG and LA-Zwitterion Ligands. Five PEGylated ligands consisting of a lipoic acid anchoring group at one end and an inert (OCH_3) or reactive functional group (COOH, NH_2 or N_3) at the other end have been synthesized, purified, and characterized following the protocols detailed in our previous reports.[54−56,79] They are LA-PEG_{750}-OCH_3 (PEG M_w = 750), LA-PEG_{550}-OCH_3 (PEG M_w = 550), LA-PEG_{600}-COOH (PEG M_w = 600), LA-PEG_{600}-NH_2 (PEG M_w = 600), and LA-PEG_{600}-N_3 (PEG M_w = 600). The LA-zwitterion ligand was synthesized using the scheme described by Kim and co-workers with a slight modification.[51,53] Here, we used two reaction steps: (1) coupling of lipoic acid to *N*,*N*-dimethyl-1,3-propanediamine using 1,1-carbonyldiimidazole to form a tertiary amine linked to LA and (2) reaction with 1,3-propanesultone; we have used *N*,*N*-dimethyl-1,3-propanediamine instead of *N*,*N*-dimethylethylene diamine as described in ref 51.

Growth of Gold Nanoclusters. The growth scheme relied on the reduction of Au(III) using sodium borohydride in the presence of pure lipoic acid, LA-PEG_{550}-OCH_3, LA-PEG_{750}-OCH_3, or LA-ZW ligands, following previously reported rationales.[38,48] In a typical reaction, 30 μmol of ligand was dissolved in 20 mL of deionized water containing 50 μL of 2 M NaOH, followed by the addition of 200 μL of 50 mM $HAuCl_4 \cdot 3H_2O$ (ratio of Au:ligand = 1:3). The mixture was stirred for 5 min; then 400 μL of 50 mM $NaBH_4$ was added dropwise. The reaction mixture was stirred for 15 h at room temperature and then purified from free ligands by applying three cycles of centrifugation/filtration using a membrane filtration device (Millipore) with a molecular weight cutoff of 10 kDa; the resulting dispersions were stored at 4 °C until further use. Growth of Au nanoparticles using LA-ZW ligands following the protocol from ref 48, is described in the Supporting Information.

***In Situ* Functionalization of AuNCs.** The functionalization of AuNCs with carboxy- or amine-terminated ligands was achieved by introducing a small fraction of reactive ligands (LA-PEG_{600}-COOH or LA-PEG_{600}-NH_2) along with LA-PEG_{750}-OCH_3 or LA-ZW (inert ligand) at the desired molar ratios prior to the reduction step; the ligand concentrations were adjusted to satisfy a final Au:$NaBH_4$:ligand ratio of 1:2:3. Because the use of $NaBH_4$ is proven to alter the integrity of azide groups,[72] introduction of LA-PEG-azide on the cluster surface was carried out postgrowth using a process referred to as extra passivation, as done in ref 48. Briefly, following growth and purification of the AuNCs capped with LA-PEG_{750}-OCH_3 prepared in 20 mL (stock reaction/solution) using a Au:ligand ratio of 1:3, the dispersion was further diluted in 5 mL of water, followed by the addition of 2.4 mL of 12.3 mM stock solution of LA-PEG_{600}-N_3 (3×10^{-5} mol of ligands); this corresponds to a 3-to-1 excess of ligands compared to gold precursor. The mixture was stirred for 3 h at room temperature and then purified from free ligands by applying three cycles of centrifugation/filtration as described above. The purified sample

was then lyophilized and characterized by FT-IR to verify the introduction of azide groups on the cluster surface.

Covalent Conjugation of Sulfo-Cy3 to Aminated AuNCs. In a typical reaction, clusters prepared with a ligand mixture containing 30% or 100% LA-PEG_{600}-NH_2 (200 μL, 10 μM) were dispersed in 800 μL of PBS buffer (pH = 8.4). Then, sulfo-Cy3 NHS ester (4.7 μL, 8.4 mM in DMSO) was added, and the mixture was stirred for four hours (the final AuNC:dye ratio used was 1:20). The AuNC-sulfo-Cy3 conjugates were purified by size exclusion using a PD10 column (GE Healthcare), then characterized using UV–vis absorption spectroscopy. The concentration of AuNCs was calculated using the extinction coefficient reported for commercially available 1.4 nm size AuNPs (ε at 420 nm = 112 000 cm^{-1} M^{-1}), which is only an approximation value.[80]

Conflict of Interest: The authors declare no competing financial interest.

Acknowledgment. We thank FSU and the National Science Foundation (NSF-CHE, #1058957) for financial support. We also thank Xin Ji, Hyon Bin Na, Laura Trapiella-Alfonso, and Dr. Lei Bruschweiler for helpful discussions and assistance with the gel experiments. The TEM work was carried out at the FSU TEM facility, funded and supported by the Florida State University Research Foundation, the National High Magnetic Field Laboratory (NSF-DMR-0654118), and the State of Florida.

Supporting Information Available: Additional experimental details on the growth of Au nanoparticles using LA-ZW, time-resolved fluorescence data analysis, effects of varying the Au-to-ligand ratio, Au-to-$NaBH_4$ ratio and functional groups on the UV–vis absorption and/or fluorescence emission, and colloidal stability tests of clusters grown using lipoic acid. This material is available free of charge *via* the Internet at http://pubs.acs.org.

REFERENCES AND NOTES

1. Jin, R. Quantum Sized, Thiolate-Protected Gold Nanoclusters. *Nanoscale* **2010**, *2*, 343–362.
2. Zheng, J.; Nicovich, P. R.; Dickson, R. M. Highly Fluorescent Noble-Metal Quantum Dots. *Annu. Rev. Phys. Chem.* **2007**, *58*, 409–431.
3. Chen, S. W.; Ingram, R. S.; Hostetler, M. J.; Pietron, J. J.; Murray, R. W.; Schaaff, T. G.; Khoury, J. T.; Alvarez, M. M.; Whetten, R. L. Gold Nanoelectrodes of Varied Size: Transition to Molecule-like Charging. *Science* **1998**, *280*, 2098–2101.
4. Apell, P.; Monreal, R.; Lundqvist, S. Photoluminescence of Noble-Metals. *Phys. Scr.* **1988**, *38*, 174–179.
5. Schaaff, T. G.; Knight, G.; Shafigullin, M. N.; Borkman, R. F.; Whetten, R. L. Isolation and Selected Properties of a 10.4 kDa Gold: Glutathione Cluster Compound. *J. Phys. Chem. B* **1998**, *102*, 10643–10646.
6. Bigioni, T. P.; Whetten, R. L.; Dag, O. Near-Infrared Luminescence from Small Gold Nanocrystals. *J. Phys. Chem. B* **2000**, *104*, 6983–6986.
7. Herzing, A. A.; Kiely, C. J.; Carley, A. F.; Landon, P.; Hutchings, G. J. Identification of Active Gold Nanoclusters on Iron Oxide Supports for CO Oxidation. *Science* **2008**, *321*, 1331–1335.
8. Lee, D. I.; Donkers, R. L.; DeSimone, J. M.; Murray, R. W. Voltammetry and Electron-Transfer Dynamics in a Molecular Melt of a 1.2 nm Metal Quantum Dot. *J. Am. Chem. Soc.* **2003**, *125*, 1182–1183.
9. Negishi, Y.; Tsunoyama, H.; Suzuki, M.; Kawamura, N.; Matsushita, M. M.; Maruyama, K.; Sugawara, T.; Yokoyama, T.; Tsukuda, T. X-ray Magnetic Circular Dichroism of Size-Selected, Thiolated Gold Clusters. *J. Am. Chem. Soc.* **2006**, *128*, 12034–12035.
10. Zhu, M.; Aikens, C. M.; Hollander, F. J.; Schatz, G. C.; Jin, R. Correlating the Crystal Structure of a Thiol-Protected Au-25 Cluster and Optical Properties. *J. Am. Chem. Soc.* **2008**, *130*, 5883–5885.
11. Pelley, J. L.; Daar, A. S.; Saner, M. A. State of Academic Knowledge on Toxicity and Biological Fate of Quantum Dots. *Toxicol. Sci.* **2009**, *112*, 276–296.
12. Wang, H. H.; Lin, C. A. J.; Lee, C. H.; Lin, Y. C.; Tseng, Y. M.; Hsieh, C. L.; Chen, C. H.; Tsai, C. H.; Hsieh, C. T.; Shen, J. L. *et al.* Fluorescent Gold Nanoclusters as a Biocompatible Marker for *in Vitro* and *in Vivo* Tracking of Endothelial Cells. *ACS Nano* **2011**, *5*, 4337–4344.
13. Wu, X.; He, X. X.; Wang, K. M.; Xie, C.; Zhou, B.; Qing, Z. H. Ultrasmall Near-Infrared Gold Nanoclusters for Tumor Fluorescence Imaging *in Vivo*. *Nanoscale* **2010**, *2*, 2244–2249.
14. Zhang, X. D.; Wu, D.; Shen, X.; Liu, P. X.; Fan, F. Y.; Fan, S. J. *In Vivo* Renal Clearance, Biodistribution, Toxicity of Gold Nanoclusters. *Biomaterials* **2012**, *33*, 4628–4638.
15. Lin, C. A. J.; Lee, C. H.; Hsieh, J. T.; Wang, H. H.; Li, J. K.; Shen, J. L.; Chan, W. H.; Yeh, H. I.; Chang, W. H. Synthesis of Fluorescent Metallic Nanoclusters toward Biomedical Application: Recent Progress and Present Challenges. *J. Med. Biol. Eng.* **2009**, *29*, 276–283.
16. Cannone, F.; Collini, M.; D'Alfonso, L.; Baldini, G.; Chirico, G.; Tallarida, G.; Pallavicini, P. Voltage Regulation of Fluorescence Emission of Single Dyes Bound to Gold Nanoparticles. *Nano Lett.* **2007**, *7*, 1070–1075.
17. Lee, T. H.; Gonzalez, J. I.; Zheng, J.; Dickson, R. M. Single-Molecule Optoelectronics. *Acc. Chem. Res.* **2005**, *38*, 534–541.
18. Wu, Z. K.; Jin, R. C. On the Ligand's Role in the Fluorescence of Gold Nanoclusters. *Nano Lett.* **2010**, *10*, 2568–2573.
19. Li, L. L.; Liu, H. Y.; Shen, Y. Y.; Zhang, J. R.; Zhu, J. J. Electrogenerated Chemiluminescence of Au Nanoclusters for the Detection of Dopamine. *Anal. Chem.* **2011**, *83*, 661–665.
20. Shang, L.; Dong, S. J.; Nienhaus, G. U. Ultra-small fluorescent Metal Nanoclusters: Synthesis and Biological Applications. *Nano Today* **2011**, *6*, 401–418.
21. Shiang, Y. C.; Huang, C. C.; Chen, W. Y.; Chen, P. C.; Chang, H. T. Fluorescent Gold and Silver Nanoclusters for the Analysis of Biopolymers and Cell Imaging. *J. Mater. Chem.* **2012**, *22*, 12972–12982.
22. Negishi, Y.; Nobusada, K.; Tsukuda, T. Glutathione-Protected Gold Clusters Revisited: Bridging the Gap between Gold(I)-Thiolate Complexes and Thiolate-Protected Gold Nanocrystals. *J. Am. Chem. Soc.* **2005**, *127*, 5261–5270.
23. Link, S.; Beeby, A.; FitzGerald, S.; El-Sayed, M. A.; Schaaff, T. G.; Whetten, R. L. Visible to Infrared Luminescence from a 28-Atom Gold Cluster. *J. Phys. Chem. B* **2002**, *106*, 3410–3415.
24. Duan, H. W.; Nie, S. M. Etching Colloidal Gold Nanocrystals with Hyperbranched and Multivalent Polymers: A New Route to Fluorescent and Water-Soluble Atomic Clusters. *J. Am. Chem. Soc.* **2007**, *129*, 2412–2413.
25. Muhammed, M. A. H.; Verma, P. K.; Pal, S. K.; Retnakumari, A.; Koyakutty, M.; Nair, S.; Pradeep, T. Luminescent Quantum Clusters of Gold in Bulk by Albumin-Induced Core Etching of Nanoparticles: Metal Ion Sensing, Metal-Enhanced Luminescence, and Biolabeling. *Chem.—Eur. J.* **2010**, *16*, 10103–10112.
26. Lin, C. A. J.; Yang, T. Y.; Lee, C. H.; Huang, S. H.; Sperling, R. A.; Zanella, M.; Li, J. K.; Shen, J. L.; Wang, H. H.; Yeh, H. I.; *et al.* Synthesis, Characterization, and Bioconjugation of Fluorescent Gold Nanoclusters Toward Biological Labeling Applications. *ACS Nano* **2009**, *3*, 395–401.
27. Jin, R. C.; Qian, H. F.; Wu, Z. K.; Zhu, Y.; Zhu, M. Z.; Mohanty, A.; Garg, N. Size Focusing: A Methodology for Synthesizing Atomically Precise Gold Nanoclusters. *J. Phys. Chem. Lett.* **2010**, *1*, 2903–2910.
28. Jose, D.; Matthiesen, J. E.; Parsons, C.; Sorensen, C. M.; Klabunde, K. J. Size Focusing of Nanoparticles by Thermodynamic Control Through Ligand Interactions. Molecular Clusters Compared with Nanoparticles of Metals. *J. Phys. Chem. Lett.* **2012**, *3*, 885–890.
29. Qian, H. F.; Zhu, Y.; Jin, R. C. Size-Focusing Synthesis, Optical and Electrochemical Properties of Monodisperse $Au_{38}(SC_2H_4Ph)_{24}$ Nanoclusters. *ACS Nano* **2009**, *3*, 3795–3803.
30. Shichibu, Y.; Negishi, Y.; Tsukuda, T.; Teranishi, T. Large-Scale Synthesis of Thiolated Au_{25} Clusters via Ligand

Exchange Reactions of Phosphine-Stabilized Au_{11} Clusters. *J. Am. Chem. Soc.* **2005**, *127*, 13464–13465.
31. Balasubramanian, R.; Guo, R.; Mills, A. J.; Murray, R. W. Reaction of $Au_{55}(PPh_3)_{12}Cl_6$ with Thiols Yields Thiolate Monolayer Protected Au_{75} Clusters. *J. Am. Chem. Soc.* **2005**, *127*, 8126–8132.
32. Shang, L.; Dorlich, R. M.; Brandholt, S.; Schneider, R.; Trouillet, V.; Bruns, M.; Gerthsen, D.; Nienhaus, G. U. Facile Preparation of Water-sSoluble Fluorescent Gold Nanoclusters for Cellular Imaging Applications. *Nanoscale* **2011**, *3*, 2009–2014.
33. Tian, D. H.; Qian, Z. S.; Xia, Y. S.; Zhu, C. Q. Gold Nanocluster-Based Fluorescent Probes for Near-Infrared and Turn-On Sensing of Glutathione in Living Cells. *Langmuir* **2012**, *28*, 3945–3951.
34. Yan, L.; Cai, Y. Q.; Zheng, B. Z.; Yuan, H. Y.; Guo, Y.; Xiao, D.; Choi, M. M. F. Microwave-Assisted Synthesis of BSA-Stabilized and HSA-Protected Gold Nanoclusters with Red Emission. *J. Mater. Chem.* **2012**, *22*, 1000–1005.
35. Liu, H. Y.; Zhang, X. A.; Wu, X. M.; Jiang, L. P.; Burda, C.; Zhu, J. J. Rapid Sonochemical Synthesis of Highly Luminescent Non-toxic AuNCs and Au@AgNCs and Cu (II) Sensing. *Chem. Commun.* **2011**, *47*, 4237–4239.
36. Huang, C. C.; Liao, H. Y.; Shiang, Y. C.; Lin, Z. H.; Yang, Z.; Chang, H. T. Synthesis of Wavelength-Tunable Luminescent Gold and Gold/Silver Nanodots. *J. Mater. Chem.* **2009**, *19*, 755–759.
37. Wang, Z. J.; Cai, W.; Sui, J. H. Blue Luminescence Emitted from Monodisperse Thiolate-Capped Au-11 Clusters. *ChemPhysChem* **2009**, *10*, 2012–2015.
38. Shang, L.; Azadfar, N.; Stockmar, F.; Send, W.; Trouillet, V.; Bruns, M.; Gerthsen, D.; Nienhaus, G. U. One-Pot Synthesis of Near-Infrared Fluorescent Gold Clusters for Cellular Fluorescence Lifetime Imaging. *Small* **2011**, *7*, 2614–2620.
39. Huang, X.; Li, B. Y.; Li, L.; Zhang, H.; Majeed, I.; Hussain, I.; Tan, B. E. Facile Preparation of Highly Blue Fluorescent Metal Nanoclusters in Organic Media. *J. Phys. Chem. C* **2012**, *116*, 448–455.
40. Huang, X.; Luo, Y.; Li, Z.; Li, B. Y.; Zhang, H.; Li, L.; Majeed, I.; Zou, P.; Tan, B. E. Biolabeling Hematopoietic System Cells Using Near-Infrared Fluorescent Gold Nanoclusters. *J. Phys. Chem. C* **2011**, *115*, 16753–16763.
41. Zheng, J.; Petty, J. T.; Dickson, R. M. High Quantum Yield Blue Emission from Water-Soluble Au_8 Nanodots. *J. Am. Chem. Soc.* **2003**, *125*, 7780–7781.
42. Bao, Y. P.; Zhong, C.; Vu, D. M.; Temirov, J. P.; Dyer, R. B.; Martinez, J. S. Nanoparticle-Free Synthesis of Fluorescent Gold Nanoclusters at Physiological Temperature. *J. Phys. Chem. C* **2007**, *111*, 12194–12198.
43. Zheng, J.; Zhang, C. W.; Dickson, R. M. Highly Fluorescent, Water-Soluble, Size-Tunable Gold Quantum Dots. *Phys. Rev. Lett.* **2004**, *93*, 077402–4.
44. Shibu, E. S.; Muhammed, M. A. H.; Tsukuda, T.; Pradeep, T. Ligand Exchange of $Au_{25}SG_{18}$ Leading to Functionalized Gold Clusters: Spectroscopy, Kinetics, and Luminescence. *J. Phys. Chem. C* **2008**, *112*, 12168–12176.
45. Wang, Y. L.; Chen, J. J.; Irudayaraj, J. Nuclear Targeting Dynamics of Gold Nanoclusters for Enhanced Therapy of $HER2^+$ Breast Cancer. *ACS Nano* **2011**, *5*, 9718–9725.
46. Xavier, P. L.; Chaudhari, K.; Verma, P. K.; Pal, S. K.; Pradeep, T. Luminescent Quantum Clusters of Gold in Transferrin Family Pprotein, Lactoferrin Exhibiting FRET. *Nanoscale* **2010**, *2*, 2769–2776.
47. Kennedy, T. A. C.; MacLean, J. L.; Liu, J. W. Blue Emitting Gold Nanoclusters Templated by Poly-cytosine DNA at Low pH and Poly-adenine DNA at Neutral pH. *Chem. Commun.* **2012**, *48*, 6845–6847.
48. Oh, E.; Susumu, K.; Goswami, R.; Mattoussi, H. One-Phase Synthesis of Water-Soluble Gold Nanoparticles with Control over Size and Surface Functionalities. *Langmuir* **2010**, *26*, 7604–7613.
49. Susumu, K.; Oh, E.; Delehanty, J. B.; Blanco-Canosa, J. B.; Johnson, B. J.; Jain, V.; Hervey, W. J.; Algar, W. R.; Boeneman, K.; Dawson, P. E.; *et al.* Multifunctional Compact Zwitterionic Ligands for Preparing Robust Biocompatible Semiconductor Quantum Dots and Gold Nanoparticles. *J. Am. Chem. Soc.* **2011**, *133*, 9480–9496.
50. Wei, H.; Insin, N.; Lee, J.; Han, H. S.; Cordero, J. M.; Liu, W.; Bawendi, M. G. Compact Zwitterion-Coated Iron Oxide Nanoparticles for Biological Applications. *Nano Lett.* **2012**, *12*, 22–25.
51. Park, J.; Nam, J.; Won, N.; Jin, H.; Jung, S.; Jung, S.; Cho, S. H.; Kim, S. Compact and Stable Quantum Dots with Positive, Negative, or Zwitterionic Surface: Specific Cell Interactions and Non-Specific Adsorptions by the Surface Charges. *Adv. Funct. Mater.* **2011**, *21*, 1558–1566.
52. Muro, E.; Pons, T.; Lequeux, N.; Fragola, A.; Sanson, N.; Lenkei, Z.; Dubertret, B. Small and Stable Sulfobetaine Zwitterionic Quantum Dots for Functional Live-Cell Imaging. *J. Am. Chem. Soc.* **2010**, *132*, 4556–4557.
53. Palui, G.; Avellini, T.; Zhan, N.; Pan, F.; Gray, D.; Alabugin, I.; Mattoussi, H. Photoinduced Phase Transfer of Luminescent Quantum Dots to Polar and Aqueous Media. *J. Am. Chem. Soc.* **2012**, *134*, 16370–16378.
54. Mei, B. C.; Susumu, K.; Medintz, I. L.; Delehanty, J. B.; Mountziaris, T. J.; Mattoussi, H. Modular Poly(ethylene glycol) Ligands for Biocompatible Semiconductor and Gold Nanocrystals with Extended pH and Ionic Stability. *J. Mater. Chem.* **2008**, *18*, 4949–4958.
55. Mei, B. C.; Susumu, K.; Medintz, I. L.; Mattoussi, H. Polyethylene Glycol-Based Bidentate Ligands to Enhance Quantum Dot and Gold Nanoparticle Stability in Biological Media. *Nat. Protoc.* **2009**, *4*, 412–423.
56. Susumu, K.; Mei, B. C.; Mattoussi, H. Multifunctional Ligands Based on Dihydrolipoic Acid and Polyethylene Glycol to Promote Biocompatibility of Quantum Dots. *Nat. Protoc.* **2009**, *4*, 424–436.
57. Ji, X.; Palui, G.; Avellini, T.; Na, H. B.; Yi, C. Y.; Knappenberger, K. L.; Mattoussi, H. On the pH-Dependent Quenching of Quantum Dot Photoluminescence by Redox Active Dopamine. *J. Am. Chem. Soc.* **2012**, *134*, 6006–6017.
58. Muhammed, M. A.; Aldeek, F.; Palui, G.; Trapiella-Alfonso, L.; Mattoussi, H. Growth of *in Situ* Functionalized Luminescent Silver Nanoclusters by Direct Reduction and Size Focusing. *ACS Nano* **2012**, *6*, 8950–8961.
59. Alberts, B. The Promise of Cancer Research. *Science* **2008**, *320*, 19.
60. Gerweck, L. E.; Seetharaman, K. Cellular pH Gradient in Tumor Versus Normal Tissue: Potential Exploitation for the Treatment of Cancer. *Cancer Res.* **1996**, *56*, 1194–1198.
61. Nam, J.; Won, N.; Jin, H.; Chung, H.; Kim, S. pH-Induced Aggregation of Gold Nanoparticles for Photothermal Cancer Therapy. *J. Am. Chem. Soc.* **2009**, *131*, 13639–13645.
62. Yu, M. X.; Zhou, C.; Liu, J. B.; Hankins, J. D.; Zheng, J. Luminescent Gold Nanoparticles with pH-Dependent Membrane Adsorption. *J. Am. Chem. Soc.* **2011**, *133*, 11014–11017.
63. Batalia, M. A.; Kirksey, T. J.; Sharma, A.; Jiang, L. H.; Abastado, J. P.; Yan, S. Q.; Zhao, R.; Collins, E. J. Class I MHC Is Stabilized Against Thermal Denaturation by Physiological Concentrations of NaCl. *Biochemistry* **2000**, *39*, 9030–9038.
64. Terry, C. A.; Fernandez, M. J.; Gude, L.; Lorente, A.; Grant, K. B. Physiologically Relevant Concentrations of NaCl and KCl Increase DNA Photocleavage by an N-Substituted 9-Aminomethylanthracene Dye. *Biochemistry* **2011**, *50*, 10375–10389.
65. Moore, R. D.; Morrill, G. A. Possible Mechanism for Concentrating Sodium and Potassium in Cell-Nucleus. *Biophys. J.* **1976**, *16*, 527–533.
66. Cooper, A. J. L.; Kristal, B. S. Multiple Roles of Glutathione in the Central Nervous System. *Biol. Chem.* **1997**, *378*, 793–802.
67. Sudeep, P. K.; Joseph, S. T. S.; Thomas, K. G. Selective Detection of Cysteine and Gglutathione Using Gold Nanorods. *J. Am. Chem. Soc.* **2005**, *127*, 6516–6517.
68. Chen, T. H.; Tseng, W. L. (Lysozyme Type VI)-Stabilized Au8 Clusters: Synthesis Mechanism and Application for Sensing of Glutathione in a Single Drop of Blood. *Small* **2012**, *8*, 1912–1919.

69. Tehrani, Z. A.; Jamshidi, Z.; Javan, M. J.; Fattahi, A. Interactions of Glutathione Tripeptide with Gold Cluster: Influence of Intramolecular Hydrogen Bond on Complexation Behavior. *J. Phys. Chem. A* **2012**, *116*, 4338–4347.
70. Mattoussi, H.; Mauro, J. M.; Goldman, E. R.; Anderson, G. P.; Sundar, V. C.; Mikulec, F. V.; Bawendi, M. G. Self-Assembly of CdSe-ZnS Quantum Dot Bioconjugates Using an Engineered Recombinant Protein. *J. Am. Chem. Soc.* **2000**, *122*, 12142–12150.
71. Volkert, A. A.; Subramaniam, V.; Ivanov, M. R.; Goodman, A. M.; Haes, A. J. Salt-Mediated Self-Assembly of Thioctic Acid on Gold Nanoparticles. *ACS Nano* **2011**, *5*, 4570–4580.
72. Scriven, E. F. V.; Turnbull, K. Azides—Their Preparation and Synthetic Uses. *Chem. Rev.* **1988**, *88*, 297–368.
73. Na, H. B.; Palui, G.; Rosenberg, J. T.; Ji, X.; Grant, S. C.; Mattoussi, H. Multidentate Catechol-Based Polyethylene Glycol Oligomers Provide Enhanced Stability and Biocompatibility to Iron Oxide Nanoparticles. *ACS Nano* **2012**, *6*, 389–399.
74. Bucher, G.; Lu, C. Y.; Sander, W. The Photochemistry of Lipoic Acid: Photoionization and Observation of a Triplet Excited State of a Disulfide. *ChemPhysChem* **2005**, *6*, 2607–2618.
75. Wu, Z. K.; MacDonald, M. A.; Chen, J.; Zhang, P.; Jin, R. C. Kinetic Control and Thermodynamic Selection in the Synthesis of Atomically Precise Gold Nanoclusters. *J. Am. Chem. Soc.* **2011**, *133*, 9670–9673.
76. Zhou, C.; Sun, C.; Yu, M. X.; Qin, Y. P.; Wang, J. G.; Kim, M.; Zheng, J. Luminescent Gold Nanoparticles with Mixed Valence States Generated from Dissociation of Polymeric Au(I) Thiolates. *J. Phys. Chem. C* **2010**, *114*, 7727–7732.
77. Huang, T.; Murray, R. W. Visible Luminescence of Water-Soluble Monolayer-Protected Gold Clusters. *J. Phys. Chem. B* **2001**, *105*, 12498–12502.
78. Grabolle, M.; Spieles, M.; Lesnyak, V.; Gaponik, N.; Eychmuller, A.; Resch-Genger, U. Determination of the Fluorescence Quantum Yield of Quantum Dots: Suitable Procedures and Achievable Uncertainties. *Anal. Chem.* **2009**, *81*, 6285–6294.
79. Susumu, K.; Uyeda, H. T.; Medintz, I. L.; Pons, T.; Delehanty, J. B.; Mattoussi, H. Enhancing the Stability and Biological Functionalities of Quantum Dots via Compact Multifunctional Ligands. *J. Am. Chem. Soc.* **2007**, *129*, 13987–13996.
80. Pons, T.; Medintz, I. L.; Sapsford, K. E.; Higashiya, S.; Grimes, A. F.; English, D. S.; Mattoussi, H. On the Quenching of Semiconductor Quantum Dot Photoluminescence by Proximal Gold Nanoparticles. *Nano Lett.* **2007**, *7*, 3157–3164.